A 300 MM APERTURE PHASE-SHIFTING FIZEAU INTERFEROMETER

P.S. Fairman, B.K. Ward, B.F. Oreb, D.I. Farrant, Y. Gilliand*, C.H. Freund, A. J. Leistner, J. A. Seckold and C.J. Walsh.

CSIRO Telecommunications and Industrial Physics, PO Box 218 Lindfield 2070 NSW Australia, Phone +61-2-94137000, Fax +61-2-94137200;
Email: philip.fairman@tip.csiro.au

*LEICA Heerbrugg Ltd, R&D Optical Metrology CH-9425 Heerbrugg Switzerland, Fax +41-71-722556.

A 300 mm aperture digital phase-shifting Fizeau interferometer (LADI) has been developed in-house for precision metrology of optical components fabricated by the Optical Workshop at CSIRO Division of Telecommunications and Industrial Physics (CTIP). This paper describes the optical and mechanical configuration of the instrument as well as its calibration and performance characteristics. Recent measurements on 250 mm diameter uncoated optical surfaces have consistently shown short-term repeatability of 0.3 nm rms from measurement to measurement and allowed absolute characterisation of these surfaces to an accuracy of a few nanometres.

Subject terms: optical interferometry; phase-shifting; precision metrology; absolute flatness.

1. Introduction

Over many years our Optical Workshop has pioneered a stable and precise optical polishing technique[1] which uses a teflon lap. This polishing process allows controlled and efficient fabrication of ultra-flat and ultra-smooth surfaces. We are now experiencing an increasing demand to produce large optical surfaces which must be finished and certified to within a few nanometres, or better, of an ideal shape. Until recently, the metrology required was a major obstacle to precision fabrication of large optical components using the teflon lap polishing method. A Fizeau interferometer[2] in combination with phase-shifting techniques[3,4] potentially offers a flexible and practical configuration for such demanding metrology. Phase shifting can achieve sub nanometre precision in fringe interpretation. However, applying this technique to the measurement of large optics still poses special problems which often seriously limit the achievable accuracy. Some of these problems include environmental effects, mechanical instability, settling time of the instrument and test optics and the mechanism for implementing the phase shifting.

In this paper we describe a Fizeau style phase-shifting interferometer which we have developed for precision metrology of optical surfaces with diameters up to 300 mm.

2. Optical Configuration

A schematic diagram of the Large Aperture Digital Interferometer (LADI) is shown in figure 1. The light source for the instrument is a temperature-controlled pig-tailed laser diode incorporating a single mode polarisation preserving fibre (SMPP fibre). A rotating diffuser (R.D.) is used to minimise coherent noise in the interferometer. The diffuser is placed in the focal plane of an aspheric collimating lens. The collimated beam is reflected off the uncoated reference surface and also off the test surface to produce two-beam interference fringes which are viewed by a TV camera with a CCD area detector. The reference flat is wedged so that the light reflected from its back surface does not reach the detector. As shown in the figure the source and the detector are slightly offset (in opposite

directions) from the optical axis of the collimator, so that a beam splitter (which would introduce aberrations) is not required to separate the diverging and converging beams. The clear aperture of the collimator and the reference flat is 320 mm in diameter, while the focal length of the collimator is 2581 mm, resulting in a f-number of f/8. The aperture stop (A.S.) near the rotating diffuser in combination with the aperture stop in front of the detector sets the upper limit for the spatial frequency response of the instrument. This is because the aperture stop in front of the diffuser sets the effective source size while the aperture stop in front of the detector acts like a spatial filter in the plane containing the Fourier transform of the interference wavefront. The focus of the TV camera lens (a 55 mm f/2.8 fixed focal length Nikon lens) is set to image the reference and test surfaces onto the 760 x 580 pixel array of the CCD camera (Pulnix model TM765, pixel size 11 μ m x 11 μ m). This imaging minimises coherent noise[5] at the detector due to scattering from dust and surface imperfections in the optics of the instrument. To further reduce the effects of coherent noise the protective glass window over the CCD array was removed.

The laser diode source is a Toshiba TOLD9140. It is coupled to a single-mode polarisation-preserving fibre which is terminated with adjustable diverging optics, allowing adjustment of f-number from 1.8 to 5. At f/1.8, a 30° diverging beam is produced which substantially overfills the acceptance angle of the collimator resulting in a near uniform light distribution across the aperture of the interferometer. The fibre ends are cleaved at an angle to improve laser stability by isolating it from reflected light.

Table 1 summarises the specifications of the laser diode source used.

3. Measurement of Phase

The phase variations in the interference pattern are measured by a phase-shifting technique. The wavelength of the laser diode is changed slightly in a sequence of equal steps and for each step the irradiance in the interference pattern is recorded by the TV camera, digitised by a 10-bit frame grabber (Matrox Pulsar board) and stored in a computer. From these stored images the phase in the interference pattern is evaluated by the computer with an appropriate phase-shifting algorithm[6]. The wavelength of the laser varies linearly with the injection current over most of its range and the current is changed through a computer programmable power supply. The wavelength step used in the phase-shifting process depends on the phase-shifting algorithm and the air gap between the reference and test surfaces. If g is the air gap between the reference and test surfaces then the phase step $\Delta\varphi$ (in radians) introduced between the interfering beams by a wavelength shift $\Delta\lambda$, is given by[8]

$$\Delta\varphi = (2\pi / \lambda^2)2g\Delta\lambda \qquad (1)$$

where λ is the nominal operating wavelength (690.7 nm). For a seven sample algorithm[7], $\Delta\varphi = \pi / 3$ and for an air gap of 40 mm, $\Delta\lambda \approx 0.001$ nm which corresponds to a change in frequency of 0.625 GHz and injection current of 0.14 mA. Six such steps are required to implement the seven sample algorithm corresponding to a total current change of about 0.84 mA. In our measurements we use a specialised averaging procedure which is explained in Section 6. This averaging procedure increases the total phase shift required to about 3π radians and correspondingly the total drive current by 50%.

The choice of an appropriate air gap g in the instrument is a compromise. The air gap should be as small as possible to minimise fringe pattern instability due to environmental effects and for good fringe contrast. However, problems due to wavelength instability and

mode hopping are reduced when the changes in injection current required for a 2π phase shift are small. This is achieved when the air gap is increased. We found an air gap of 40 mm to 100 mm to be an acceptable working range.

Changing the current of the laser diode can introduce potential problems[8], including laser temperature change and mode hops. These can result in undesirable wavelength instability. To minimise the temperature variation, the laser diode is mounted on a heat sink whose temperature is controlled by a Peltier cooler (TEC in figure 1). During a data acquisition cycle the wavelength shifting is carried out rapidly (in less than a second) in comparison to the time constant of the temperature controller. To minimise the occurrence of mode hops, an optimal case temperature and injection current region were determined experimentally through observation of the interference pattern as a function of these parameters. The case temperature was adjusted in 0.5 °C steps from 19 °C to 25 °C (the total temperature range available from our temperature control electronics). At each temperature the current to the diode was slowly tuned from 50 to 55 mA in 0.1 mA steps and an intensity profile of the interferogram recorded at each current setting. The profiles were then combined in an animation and viewed to determine the most stable temperature and current regions. This indicated the most stable temperature region to be 23.5 °C - 24.0 °C, with the preferred current range of 52 - 53 mA.

Changes in the injection current also affect the laser power. This introduces errors in the calculated phase of the interferogram which are algorithm dependent. However, computer simulation of this effect for our seven sample algorithm showed a negligible level of error.

4. Mechanical Configuration

The LADI instrument, shown in figure 2, is built on a modified milling machine base. The illumination and the detection components are mounted on a fixed platform at the back of the instrument and half-way up its height. The collimator and the reference flat are mounted horizontally on a non-movable part of the instrument slightly below and in front of the illumination and detection optics. The test optics is also mounted horizontally on an adjustable platform directly below the reference flat. The height of the platform may be adjusted through a range of 190 mm. It can also slide forward to allow placement and removal of the test optics and it can be tilted to allow alignment with the reference surface. A coarse tilt adjustment is provided by three mechanical screws and a fine adjustment by three-voltage driven PZT stacks. The diverging beam from the laser source is directed to the collimator via a fold-back mirror mounted at the top of the instrument. This mirror is supported by a truss assembly constructed of sand filled metal tubes (25 mm diameter), lined with lead to reduce vibration. The truss assembly and the fold-back mirror are then covered by a metal cylinder (450 mm diameter) to reduce air currents and dust. To aid in the alignment of test optics with respect to the reference surface, a beam splitter mounted near the base of the cylinder (not shown in figures 1 and 2) can be manually flipped into the path of the diverging beam and the deflected reference and test beams viewed from the front of the instrument. Once an interference pattern has been established (by aligning the two beams), the beam splitter is swung out of the beam path and the interference pattern viewed on the TV monitor.

Figure 3 shows a photograph of the instrument in our metrology laboratory. The height of the instrument is about 2.5 m and it weighs around 1000 kg. The instrument is isolated from the concrete floor by four rubber pads. The laboratory is temperature- and humidity-controlled (21.5 ± 0.1 ^{0}C, 50 $\pm 5\%$). The warm-up time of the instrument is about 20

minutes after which a drift rate of less than 0.1 fringe per 3 minutes is achieved for test surface measurements. During measurements the air gap and the test optic are shrouded by a retractable opaque curtain. A thermistor sensor is placed in the air gap area and the temperature recorded continuously on a paper chart recorder. The temperature in the air gap region varies typically by less then 0.05 ^{0}C over periods of several hours.

5. Calibration of the Instrument

The form of the reference surface and the aberrations in the interferometer must be characterised absolutely to enable precision measurement of test surfaces to be made. This process generates a reference data file (RDF) which is stored in the computer and subtracted from a measurement of a test surface to obtain the absolute form or shape of the test surface. The generation of the RDF and instrument error analysis will be the subject of a separate publication, however the RDF procedure, which consists of four steps, is briefly outlined below. In the first step the absolute surface form or figure of the reference surface is measured by the intercomparison of three flats. In the second step the sag of the reference surface due to gravity is measured. In the third step the fine structure or ripple on the reference surface is measured with the aid of a test flat which was translated to many positions with respect to the reference flat. Finally, in the fourth step, the measurements of the previous three steps are combined to produce the RDF.

5.1 *Surface Figure Determination*

The conventional method involving the intercomparison of a set of three surfaces, taken two at a time[9], was used to obtain the surface errors (deviations from flatness) along two perpendicular diameters of the reference surface (surface C) and of two other test surfaces (surfaces B and A). The reference flat (C) and the two test flats (B and A) were fabricated to be nominally the same (i.e. physical diameter of 350 mm, thickness 90 mm, a groove cut around the circumference, a wedge of 20' between the two sides, a good quality flat surface on one side and a lesser quality surface on the back side). During this three-flat measurement the test and reference flats were mounted in a horizontal configuration inside a collar mount with six-finger support.

Figure 4 shows one of the flats mounted in the external collar mount. The black metal ring has three sets of mounting brackets each consisting of a two-finger support. This ring and the finger supports are essentially identical to the support structure for the reference flat in the LADI. Around the edge of the flat a groove can be seen into which the fingers engage and support the optic.

From the four measurements described above, two perpendicular diametral profiles (without the gravitational sag component) are obtained for each of the three flats.

The next step involved the generation of additional absolute profiles along the reference flat C, by a series of measurements of C against B with C translated and rotated between subsequent measurements. The two perpendicular diametral profiles on flat B measured above were used as the absolute reference profiles for the additional profiles along C. For these measurements the flat B was mounted in the LADI instrument (where the reference surface C normally sits) and the reference flat C was mounted externally on the LADI test optic table. The flat C was supported uniformly over its back surface by sitting it on a velveteen covered foam rubber layer above a precision ground flat metal plate. By mounting the flat C in this way the sag due to gravity is removed.

A set of 30 equally spaced (~10 mm) x-direction profiles were generated by translating C in the y-direction and 30 equally spaced y-direction profiles by translating C in the x-direction . Likewise a set of additional diametral profiles along C was measured by rotating the flat C in equal increments of 20°. In the measurement of these additional profiles, the reference flat was moved between subsequent measurements and this introduced random offset (piston) and tilt terms in each of the measurements. From each of the C profiles, the absolute B profile was subtracted to give the absolute C profiles. These profiles from the x, y and angular scans were then tied together by a specialised routine to compensate for their random offsets and tilts.

5.2 *Sag Due to Gravity*

The sag in the reference surface was measured using the following two step approach. Test flat B was mounted in the LADI instead of the reference flat and the reference flat C was measured in two configurations with respect to B. Firstly C was suspended in the external collar where its sag was nominally the same as for the B (in reference mount) and secondly, C was lowered out of the collar mount onto a uniform foam support as described in section 5.1 above. These two measurements were subtracted from each other to obtain the sag map of the reference flat. The assumption made here was that the sag in C as mounted in the external collar is the same as it is when mounted in the LADI reference surface mount. To add confidence to this assumption the sag in the reference surface was modelled by a finite-element analysis program. The results of the finite-element analysis showed a slight asymmetry of sag in the two perpendicular directions due to the presence of a wedge between the two sides and also an effect near the edge of the flat due to the six-finger support. This was in agreement with the measured sag. The predominant terms in the measured sag are a power term of about 30 nm and astigmatism of about 7 nm over an aperture of 293 mm. Figure 5 shows the measured sag after power and astigmatism have been removed leaving predominantly the effect of the six-finger support around the perimeter of the flat. The print-through can be seen to be slightly larger at the bottom of the phase map (corresponding to the thick end of the wedge) than at the top of the map (thin end of the wedge).

5.3 *Surface Ripple*

The measurement of the fine spatial structure or ripples over the reference surface, with a spatial wavelength shorter than about 50 mm was measured by an averaging method[10] described elsewhere. For these measurements the reference surface C was mounted in the LADI's reference mount and the test flat (A) was measured against C in a number of relative positions. The flat A was translated in a series of random size steps (from 0.5 mm to a maximum of 50 mm) in both the x and y directions and an interferogram recorded for each position. A set of 60 such interferograms was recorded and averaged to smooth out the small scale irregularities contributed by the test surface A. Zernike polynomials were then fitted to the averaged data file and a surface generated from the polynomial coefficients. This surface was then subtracted from the averaged data file leaving a residual which represents the fine structure in the reference wavefront.

Figure 6 is a grey scale plot of the small scale irregularities over an aperture of 250 mm. The bottom part of the figure shows a horizontal diameter profile across this phase map.

5.4 *Generating the RDF*

The measurements in sections 5.1 to 5.3 above need to be combined to produce an RDF for the instrument. The procedure for this is as follows:

- Combine the two diametral perpendicular profiles of C with the additional profiles generated (section 5.1) into one data file. This data file is then smoothed to remove small scale irregularities by fitting a Zernike polynomial surface to the data. This generates the "surface figure" map for the reference wavefront. For the measurements presented in this paper (see section 8) the "surface figure" map was not included in the RDF (but will be presented in the future publication related to the generation of the RDF). However the deviation from flatness of the reference flat C along a number of diameters is less then 2 nm[11] and this deviation has been factored in the measurement uncertainty estimates specified in section 8 below.
- To the surface figure map add the sag map measured in section 5.2 above.
- Finally add the small scale irregularities file derived in section 5.3.

The resultant data file is the required RDF.

6. Software and data analysis

There are two main software packages that are used on LADI. The first is an in-house developed program (WinPulsar) for setting up a measurement (alignment of test optic), calibration of wavelength shifting, data acquisition, phase calculation, phase unwrapping and data format conversion. An important component of this software is a specialised averaging routine. This routine allows the phase-shifting algorithm to be applied with a programmable starting phase. In a typical measurement sequence the algorithm is applied n times (where n is an integer) with the starting phase varied by π/n radians between successive applications. The starting phases of the first and last applications are then separated by $(n-1)\pi/n$ radians. For each application of the phase shifting algorithm a phase map is evaluated and then all the n phase maps are averaged. This method of averaging is very effective in smoothing out phase errors (eg. second harmonic errors) due to random fringe drift/movement and miscalibrations in the phase shifter.

WinPulsar also allows a number of different phase-shifting algorithms to be used and the time delay between phase steps to be varied.

The second program used is a commercial package (Vision from Veeco Corp.[12]) which allows a comprehensive analysis of the phase data based on Zernike polynomials. Both programs run under Windows 95 on an Intel® processor personal computer.

Since the optics used in the LADI are not perfect (eg. both the collimating lens and the reference flat surfaces have a small number of defects such as digs and scratches and there is a hot spot in the middle of the collimator), a software procedure was used to mask out these imperfect regions over the measurement aperture. The software mask was generated by firstly measuring a high quality test flat on the LADI (see Section 7 for measurement procedure). During the phase calculation with the phase-shifting algorithm the fringe modulation threshold parameter was set to a high value (65%). This allowed the phase at any point (pixel) in the interferogram with an unacceptably low fringe contrast to be identified and set to a default value. Zernike polynomials were then fitted to the phase map of the interferogram and the Seidel terms removed from the phase map leaving a residual (higher spatial frequency) phase map. This residual map was then filtered and thresholded to obtain a binary mask which identified clearly the defective areas in the LADI aperture. This mask is referred to as the "bad pixel mask" and is applied to all the measurements on the LADI. The effect of applying the mask to a phase map of an interferogram is to set the value

of the phase at the defective sites to a "BAD" value and leave the rest of the interferogram unchanged. The total area affected by this mask is less then 1% of the LADI aperture. Figure 7 shows the "bad pixel mask".

7. Measurement procedure

In a typical measurement the test optic is placed on the extended test optic table with the underside of the optic resting on a black velveteen cloth stretched over a 4 mm thick foam rubber layer. This support provides effective isolation of the test optic from the table top and results in negligible distortion of the optic due to mounting. The table top is then retracted into its measurement position and the air gap adjusted to the desired nominal position by moving the table top up or down as required. The beamsplitter is then manually swung into the beam to aid in alignment of the test surface to the reference surface. The test optic is then tilted using the coarse tilt adjustment of the table top until an interference pattern between the reference and the test surfaces is obtained as seen through an eyepiece aligned to the beamsplitter. The beamsplitter is now retracted and the interference pattern viewed on the monitor through the WinPulsar software. With the aid of a software positioning target superimposed on the interference pattern display, the test optic is manually translated and rotated (along with the foam rubber and velveteen support) until aligned with the target. This adjustment ensures that the test optic is appropriately aligned with the optical axis of LADI and the detector array. It also allows comparisons of measurements on a given optic made at different times. The coarse tilt adjustment is then applied again until a small number of fringes remain in the interference pattern. The curtain is now drawn around the air gap and the test optic area and the instrument allowed to settle prior to taking the measurement. The settling period depends on many factors including the handling and thermal history of the test optic, the type of measurement required (surface figure or wavefront propagating through the test optic), the dimensions of the test optic and the level of accuracy required for the measurement. For best accuracy the instrument (with the test optic) is allowed to settle overnight even though in most cases a two hour period is adequate.

Just prior to the measurement the effective air gap or path difference between the reference and test wavefronts is determined through a phase-shift calibration routine which changes the laser wavelength by an amount that produces one fringe shift in the interference pattern. This calibration is then used to set the laser diode current steps in the implementation of the phase-shifting algorithm.

Once the phase-shifter has been calibrated the fringes are fluffed out or reduced to a minimum number with the fine tilt adjustment and a number of measurements are recorded. Typically, one measurement consists of an average of up to ten sets of individual phase maps recorded as described in section 6. The starting phase is offset for each application of the phase-shifting algorithm. The stability of the recorded data is checked by subtracting the phase maps of each measurement. Typically an rms difference of less then 0.5 nm is obtained when the instrument and its environment are stable. An unacceptable measurement is identified as one which has a larger or uncharacteristic rms difference (usually larger than 1.0 nm) with respect to the other measurements. The phase maps of the acceptable measurements are then all averaged and the resulting phase map stored as the raw measurement for the test wavefront. From this stored phase map the RDF of the instrument is subtracted and the bad pixel mask applied with the Veeco Vision software. This is then the final phase data representing the measurement.

8. Performance and measurement results

8.1 *Performance and specifications*

The typical short term rms repeatability between two measurements over an aperture of 293 mm is better than 0.5 nm and better than 0.3 nm over a 250 mm aperture. The uncertainty in absolute measurements is the result of many sources of errors. The major sources include the errors in deriving the RDF, the distortion of the reference flat by its mount which is not adequately represented in the RDF, errors in repositioning the reference flat, instrument retrace errors (important for non null measurement configurations where a number of fringes are present), geometric distortion and long term stability of the RDF calibration. Our current estimates of these uncertainties over an aperture of 293 mm include:

Power = 2.6 nm
Astigmatism = 5.4 nm
Coma = 1.3 nm
Spherical Aberration (SA3) = 3.9 nm

The longer term repeatability is generally much better than these uncertainties. Typically the differences between two measurements (separated by several months, with each measurement being an average of up to ten separate measurements) on the same optical surface appear as follows:

Change in power < 2 nm
Change in astigmatism < 1.5 nm
Change in coma < 0.8 nm
Change in SA3 < 0.8 nm.

The pixel size on the test surface is 0.5005 ± 0.0024 mm in the x-direction and 0.5233 ± 0.0024 mm in the y-direction. When considered with the maximum imaged aperture of 293 mm, the spatial frequency response of the instrument extends from about 1 cycle/mm (Nyquist limit) to 0.0034 cycles/mm (aperture limit). The pixel size or image magnification was measured with the aid of a precision magnification target[13]. The target consists of a series of concentric squares (of different dimensions up to 300 mm x 300 mm) accurately drawn on a mylar based film emulsion by a light pen plotter. The squares are defined by black lines on a transparent background. The dimensions and spacing of these squares were accurately measured by a travelling optical microscope instrument. The target was placed on a sheet of white paper resting on a test flat in the LADI with the air gap adjusted to about 40 mm. The target was then illuminated with white light from the side of the air gap and its image recorded by the TV camera of the LADI. The dimensions of a number of squares were then determined in the image to sub-pixel resolution. These dimensions in pixels were then compared to the corresponding actual dimensions in mm from the microscope measurements of the target to get the camera magnification and the pixel sizes in both the x and y directions. The magnitude of the pixel size uncertainty is very important when it comes to determining the radius of curvature of a test wavefront (see section 8.2 below).

8.2 *Measurement results*

LADI has been used routinely to measure not only nominally flat surfaces but also wavefronts with a large radius of curvature (ROC). We have recently fabricated and measured[11] a number of substrates for the Laser Interferometer Gravitational wave Observatory[13] (LIGO) project.

8.2.1 *Flat surfaces*

Figures 8 shows the result of a recent measurement on a LIGO mirror substrate, which was polished on our teflon lap[1]. The figure shows the surface topology of the test surface (after the RDF of the instrument is subtracted) over an aperture of about 240 mm. The surface shows an rms value of 1.5 nm corresponding to the following Seidel terms:

Power = - 0.7 nm (convex)
Astigmatism = 2.8 nm
Coma = 2.8 nm
SA3 = 14 nm

After removal of tilt, power and astigmatism, the rms residual of the surface is 1.3 nm. The uncertainty in this measurement and the other measurements presented below can be deduced from the uncertainties quoted in 8.1 above.

8.2.2 *Curved surfaces*

Some substrates in the LIGO project have curved surfaces which had to be fabricated and certified to tight tolerances (eg the End Test Mass ROC = 7400 ± 220 m). These surfaces were measured in the normal test position on the LADI. In essence these measurements allow absolute calibration of the ROC (with respect to the RDF) with an accuracy limited by the uncertainty of measurement specified in 8.1 above.

Figures 9a and 9b show a measurement on one of these curved surfaces. The Seidel terms for this measured wavefront over a 240 mm aperture are (see figure 9a):

Power = 993 nm (concave) corresponding to a ROC of 7250 m
Astigmatism = 4.1 nm
Coma = 2.0 nm
SA3 = 4.9 nm

The rms residual of the wavefront with Tilt, Power and Astigmatism removed (as shown in figure 9b) is 0.8 nm. A considerable proportion of this rms value is the measurement noise characterised by the circular bands in the phase map. These bands are caused by movement of the fringes in the original interferogram during the measurement and due to any miscalibration in the phase-shifting.
The bottom part of figures 9a and 9b show diametral profiles along the corresponding phase maps.

For the measurement of this LIGO surface, (whose nominal ROC is 7400 m), the measurement uncertainty in ROC (over an aperture of 240 mm) is estimated to be ± 75 m based on root sum squared (RSS) contributions of pixel size uncertainty and uncertainties in power, astigmatism, coma and spherical aberration (see figures given in 8.1 above). The major component of this total uncertainty is due to the pixel size uncertainty which accounts for about ± 62 m.

8.2.3 *Transmitted wavefronts*

It was also necessary to measure the transmitted wavefront on some substrates and to determine the ROC of its quadratic or power component.

For the transmitted wavefront, two separate measurements were performed. Firstly, one surface of the substrate was measured (side 1 nearest to the reference) then the optic was turned over so that the other side (side 2) was nearest to the reference. A second measurement was then made of the wavefront transmitted through side 2 propagating through the substrate , reflected off side 1 and exiting from side 2 (a double pass arrangement). The two separate measurements were then combined (by flipping one phase

map about the *y* axis, adding the resultant to the other phase map and rescaling for a single pass) to produce a single pass transmitted wavefront.

Figure 10 shows a transmitted wavefront measurement (procedure as described above) on one of the LIGO substrates (Beam Splitter) over an aperture of 240 mm. The substrate is 40 mm thick. This phase map includes the shape (surface figure) of both sides of the substrate and the refractive index inhomogeneity of the material (Suprasil - fused silica with low variation in bulk index of refraction and a low concentration of OH, supplied by Heraeus). The Seidel terms for this measured wavefront are:

Power = - 4.8 nm (convex)
Astigmatism = 8.6 nm
Coma = 5.5 nm
SA3 = 27.6 nm

The rms residual of the wavefront with Tilt, Power and Astigmatism removed is 2.6 nm. Overall, this measurement represents a combination of excellent material homogeneity and precision fabrication effort.

9. Conclusion

The LADI instrument described above is now being used routinely for precision metrology of optical components. A number of inter-comparisons have been carried out on optics measured by other groups with instruments of comparable precision and the uncertainties quoted above, we believe, are justifiable. We intend to continue work on the RDF generation, the assessment of measurement uncertainties and improvements to the instrument such as the performance of the laser diode source.

10. Acknowledgment

We are grateful to the many members of the CSIRO who have contributed to the development of LADI. In particular the mechanical design and fabrication work of P. Lennox, M. Ghaffari and S. Strachan is gratefully acknowledged as is the assistance of M. Suchting. Thanks also go to G. Forbes for the ray tracing work and helpful discussions. We would also like to thank the staff at Caltech involved with the LIGO project for the discussions relating to various measurements.
The collimator lens was fabricated by the late Bill James of James Optics.

References

1. A.J. Leistner, "Teflon polishers: their manufacture and use," *Appl. Opt.* **15** (2), 293-298 (1976).
2. J. Chen and K. Murata, "Digital phase measuring Fizeau interferometer for testing of flat and spherical surfaces," *Optik* **81** (1), 28-32 (1988).
3. K. Creath, "Phase measurement interferometry techniques", *Progress in Optics*, **26**, 349-393 (1988).
4. J.E. Grievenkamp and J.H. Brunning, "Phase shifting interferometry," Chap. 14 in *Optical Shop Testing, Second Edition*, Ed D. Malacara John Wiley and Sons (1992).
5. P. Hariharan, "Interferometric measurements of small-scale surface irregularities: sources of errors," *Opt. Eng.* **36** (8), 2330-2334 (1997).
6. K Hibino, B.F. Oreb, D.I. Farrant. and K.G. Larkin, "Phase shifting algorithms for nonlinear and spatially nonuniform phase shifts," *JOSA A* , **14**, 4, 918-930 (1997).
7. Larkin K.G. and Oreb B.F., "Design and assessment of symmetrical phase shifting algorithms," *JOSA A* **9** (10) 1740-1748 (1992).

8. P.Hariharan, "Phase-stepping interferometry with laser diodes. 2: Effects of laser wavelength modulation," *Appl. Opt.* **28** (10) 1749-50 (1989).
9. C.J. Wyant, "Absolute optical testing: better accuracy than the reference," *Photonics Spectra,* 97-101, March (1991).
10. P. Hariharan, "Optical flat surfaces: direct interferometric measurements of small-scale irregularities," *Opt. Eng.* **35** (11), 3265-3266 (1996).
11. C.J.Walsh, A.J.Leistner, J.Seckold, B.F.Oreb, D.I.Farrant, "Fabrication and Measurement of Optics for LIGO," submitted to *Appl. Opt.*
12. Veeco Inc. " Vision" software, 2650 East Elvira Rd Tucson , Arizona 85706 USA. Mention of this product does not constitute endorsement by CSIRO.
13. B.F.Oreb, K.G.Larkin, P.Fairman and M.Ghaffari, "Moire based optical surface profiler for the minting industry", *SPIE Proc.* **1776**, 48-57, SPIE Conf. on Interferometry: Surface Characterization and Testing (1992).
14. S.Whitcomb, G.Billingsley, J.Carri, A.Golovitser, D.Jungwirth, W.Kells, H.Yamamoto, B.Bochner, Y.Hefetz, P.Saha, R.Weiss, "Optics Development for LIGO," LIGO publication LIGO-P960044-CO-D, presented at TAMA Workshop (1996).

http://www.ligo.caltech.edu/

Figure and table captions

Table 1 Pig-tailed Laser diode specification

Figure 1 LADI Schematic Diagram

(Legend: A.S. – Aperture Stop, N.D.F. – Neutral Density Filter, R.D. – Rotating Diffuser, SMPP – Single Mode Polarisation Preserving Fibre, TEC – Thermo Electric Controller)

Figure 2 LADI Mechanical Drawing

Figure 3 LADI in the Laboratory

Figure 4 Test flat in the Collar Mount

Figure 5 Effect of mount on reference surface

Figure 6 Fine structure component of the RDF

Figure 7 Bad pixel mask

Figure 8 Phase map of a LIGO Fold-back Mirror surface

Figure 9 Phase map of a LIGO End Test Mass surface
(a) Complete phase map with only the Tilt removed
(b) Phase map with Tilt, Power and Astigmatism removed

Figure 10 Transmission phase map of a LIGO Beam Splitter

Table 1 Pig-tailed Laser diode specification

Parameter	Units	Spec.	Measured
Coherence Length	m	≥ 5.0	
Polarisation Ratio	dB	≤ -17	-20.0
Fibre Back-reflection Isolation	dB	-45	
Output Beam Roundness	%	≤ 90	
Operating Wavelength	nm	685 ± 10	690.7
Spectral FWHM	nm	NA	0.25
Optical Power	mW	5.0	5.00
Operating Current	mA	NA	55.6
Monitor Current	mA	NA	0.049
Maximum Optical Power	mW	≥ 5.0	7.71
Operating Current (max.)	mA	NA	64.1
Monitor Current (max.)	mA	NA	0.075
Wavelength/Current tuning	nm/mA	NA	0.007
Output Coupler Dimensions	mm	12.7x25	
Full Angle Output Beam	deg.	30	30

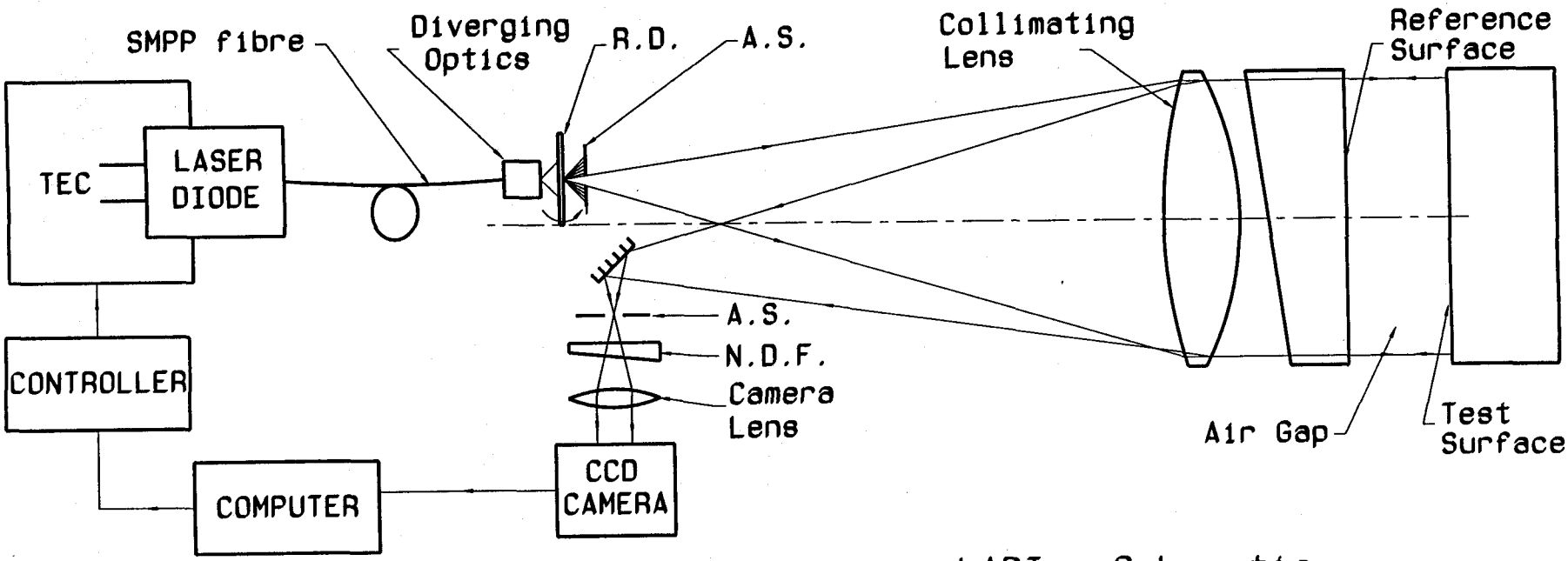

LADI - Schematic

FIGURE 1

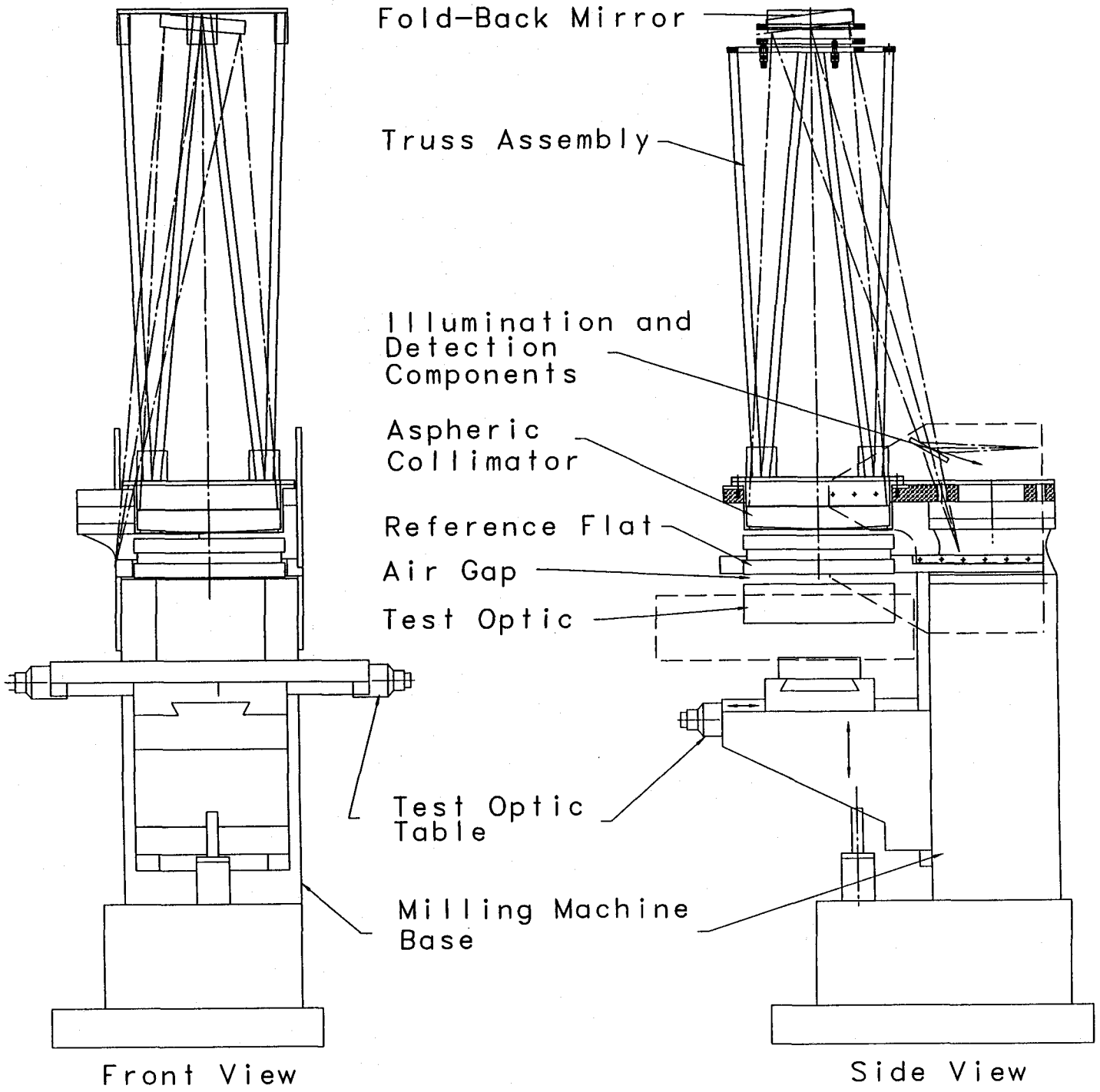
Fold-Back Mirror
Truss Assembly
Illumination and Detection Components
Aspheric Collimator
Reference Flat
Air Gap
Test Optic
Test Optic Table
Milling Machine Base
Front View
Side View

FIGURE 2

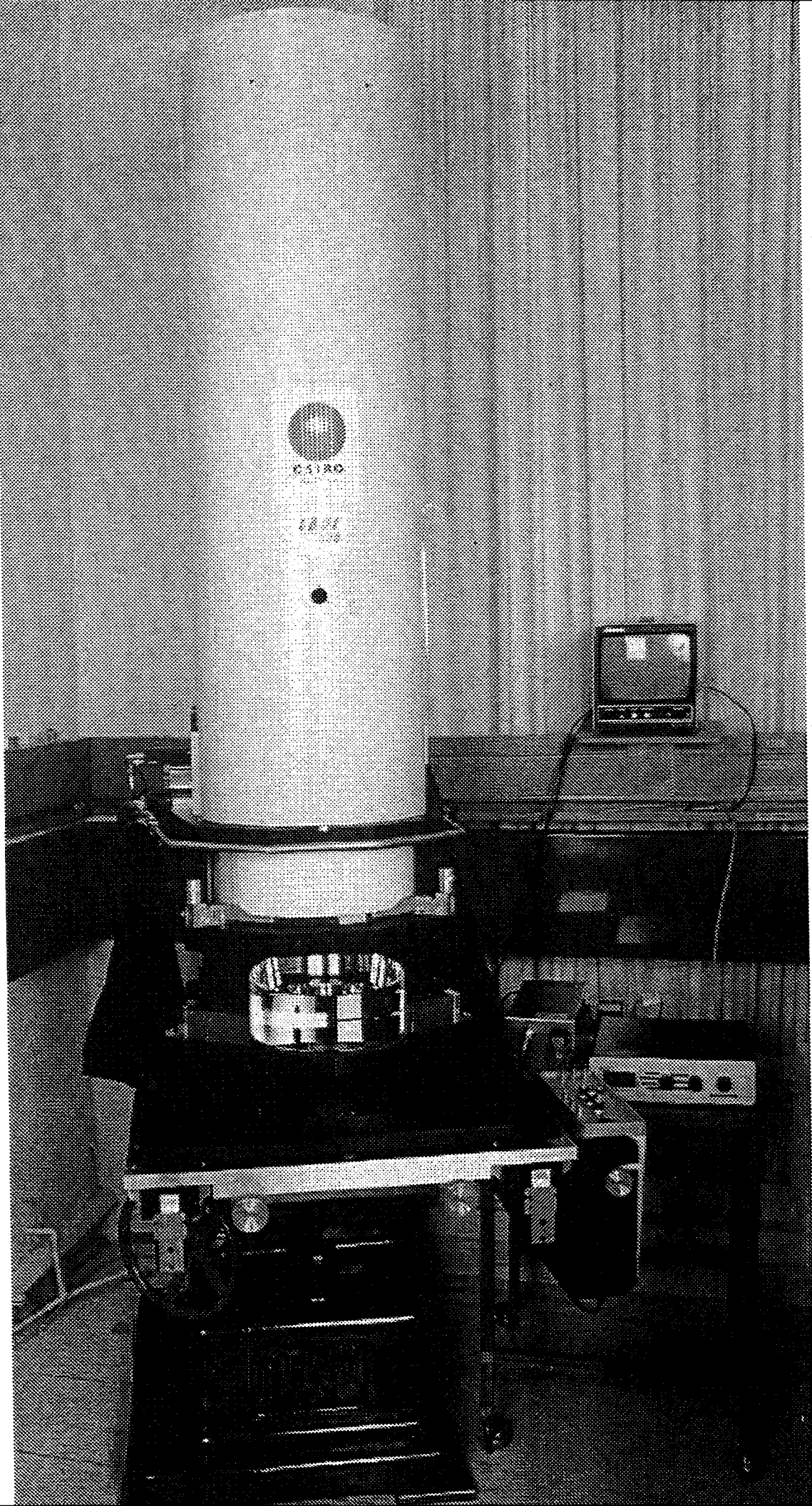
CSIRO

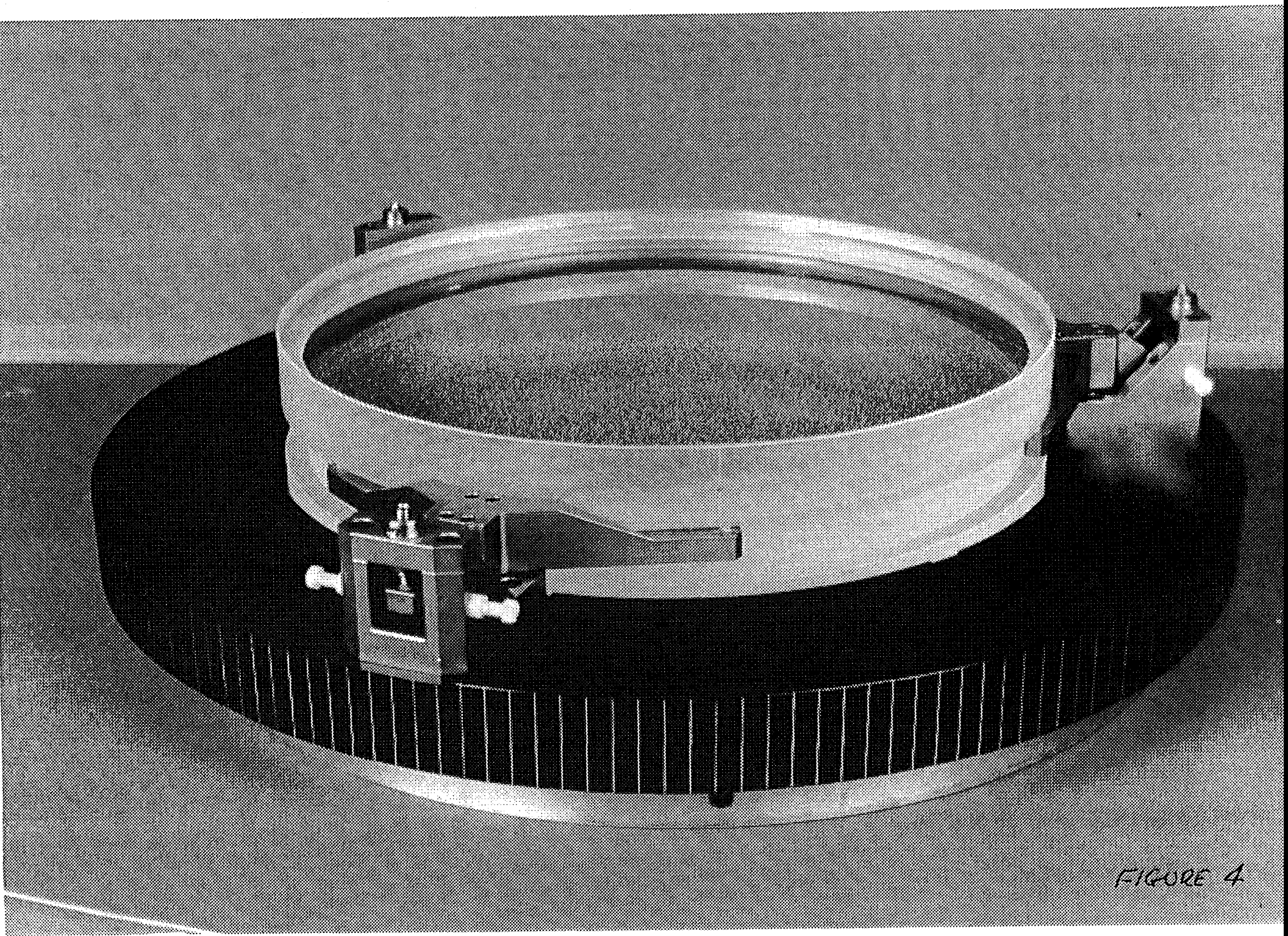

FIGURE 4

Surface Deformation Data

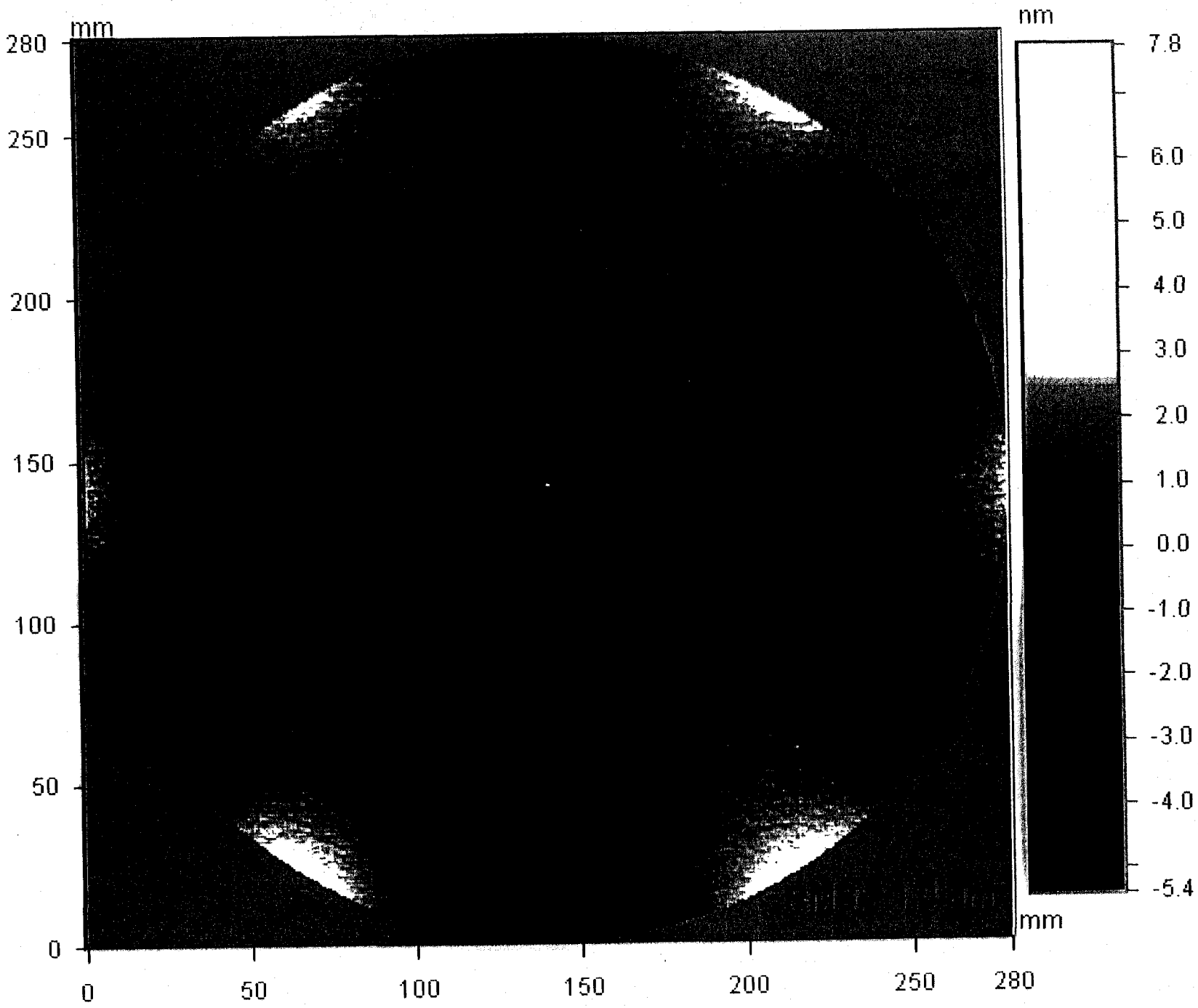

FIGU

Reference Data

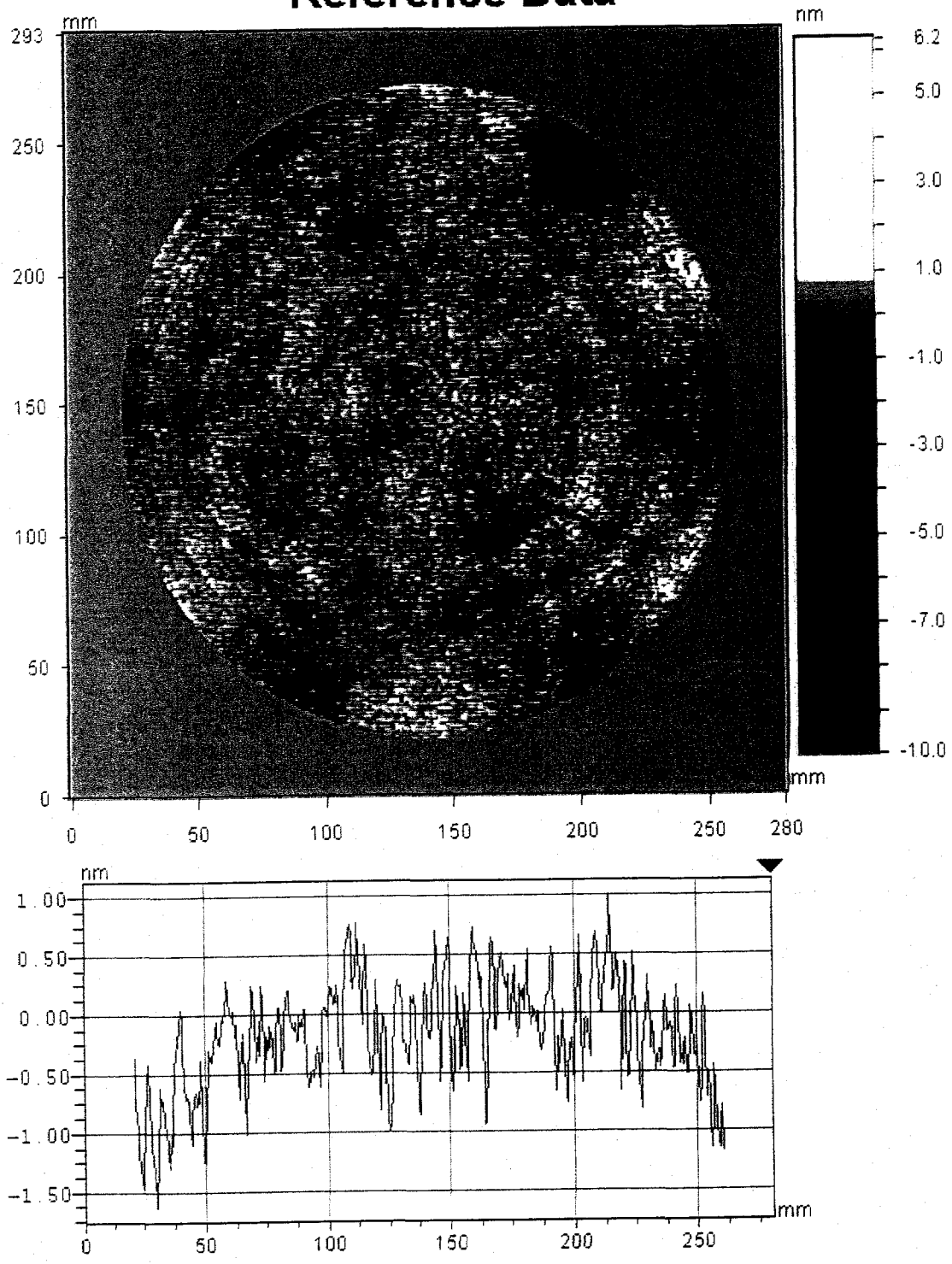

FIGURE

Surface Data

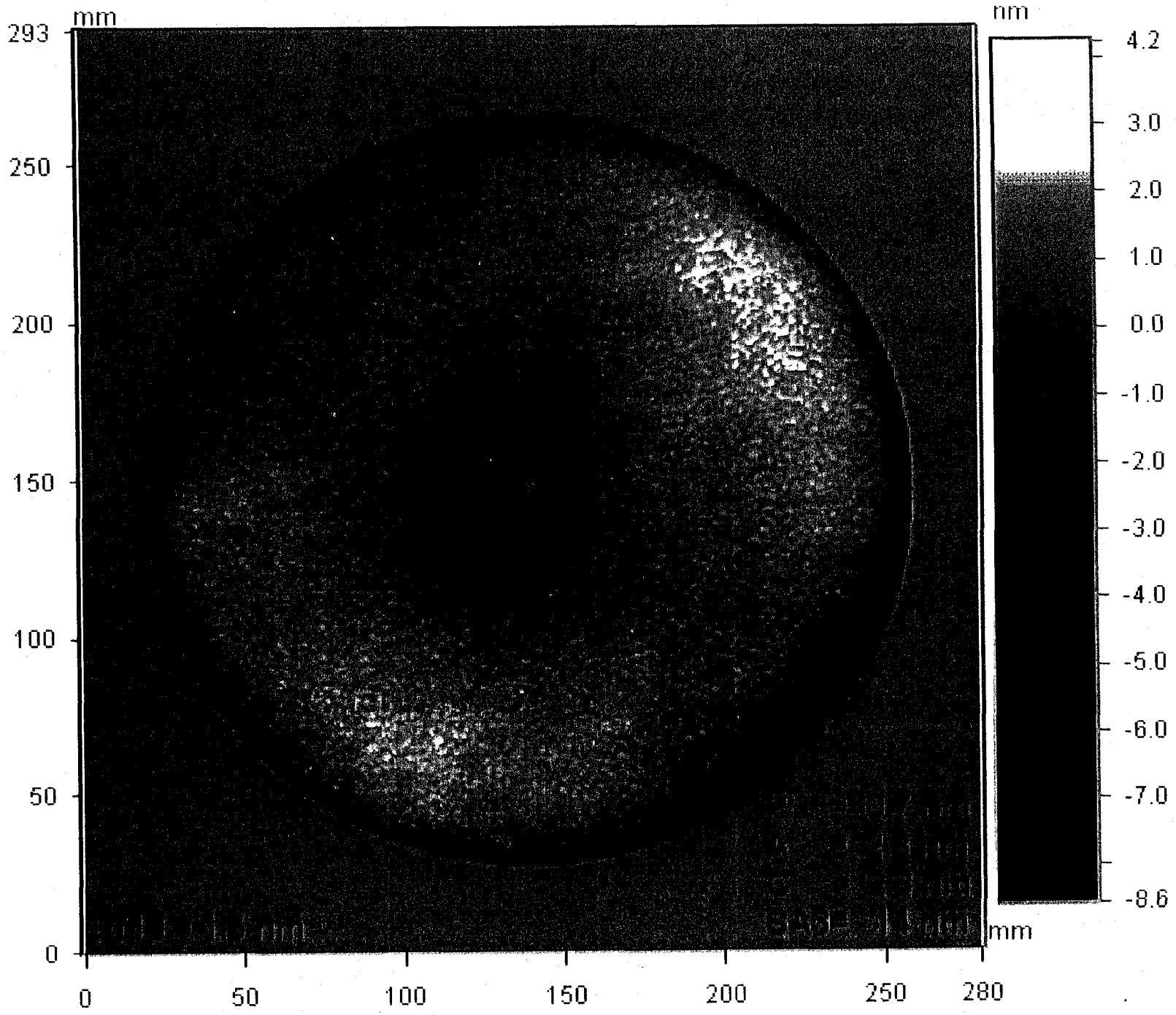

FIGURE

Surface Data

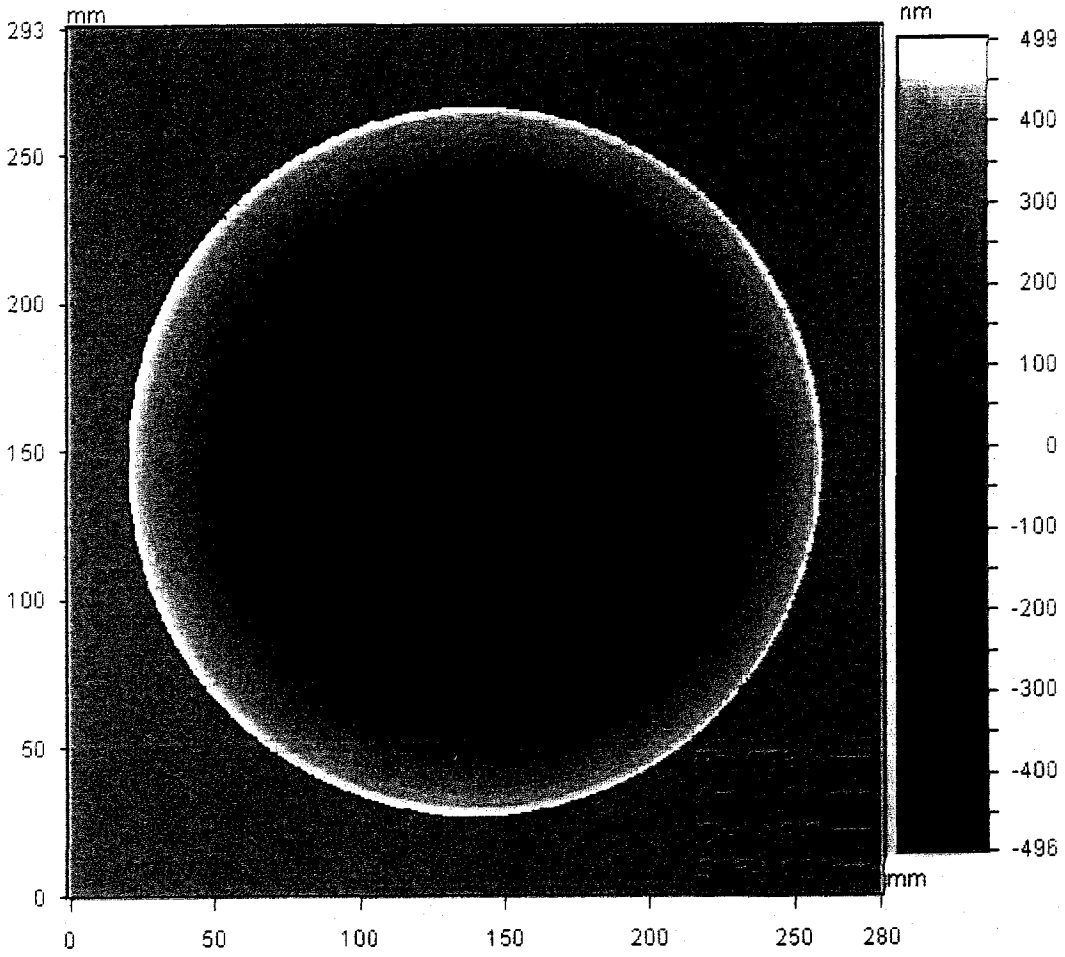

Y Profile

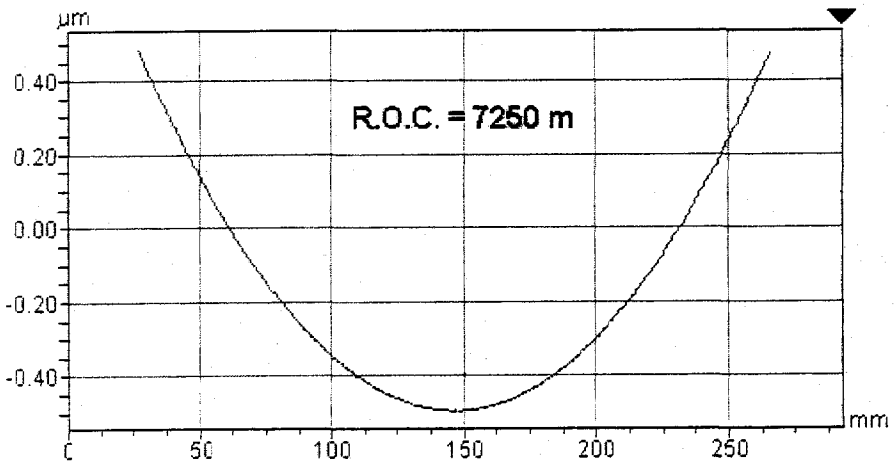

Surface Data

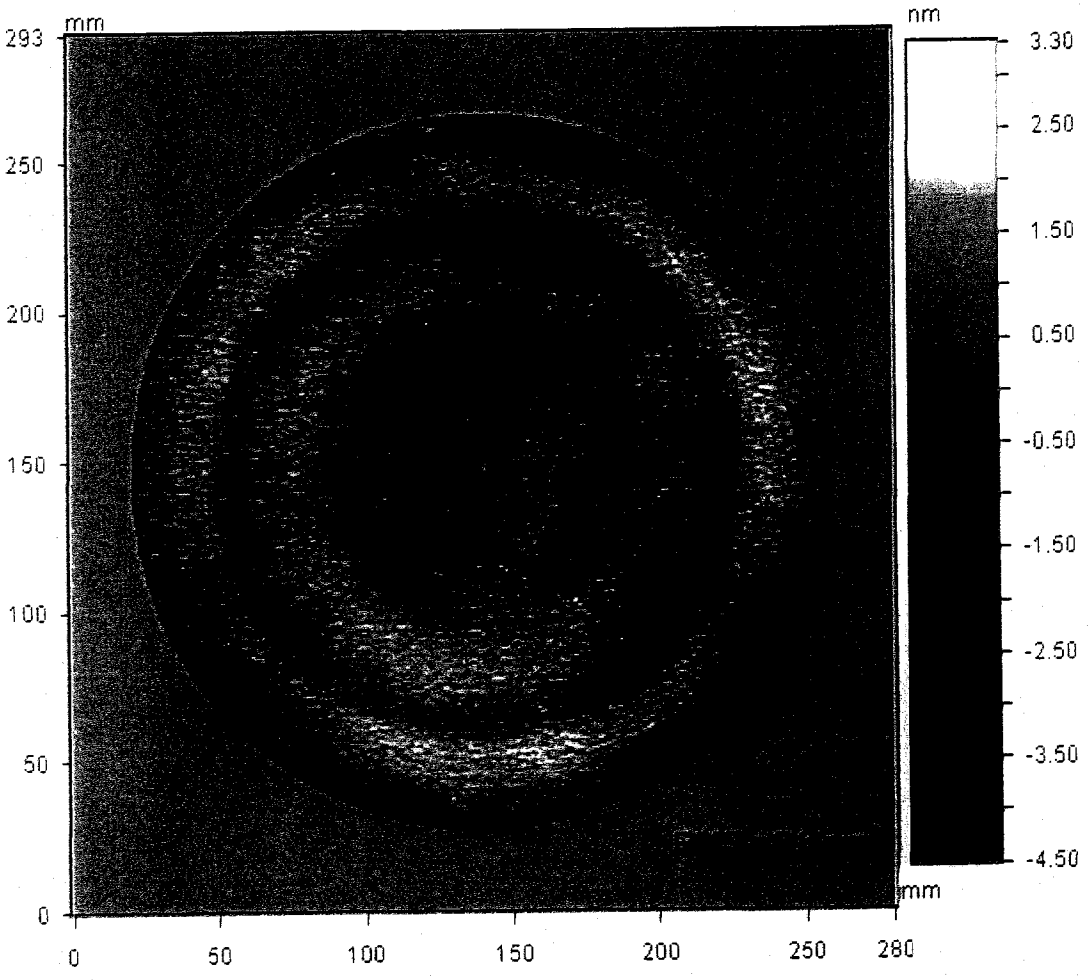

X Profile

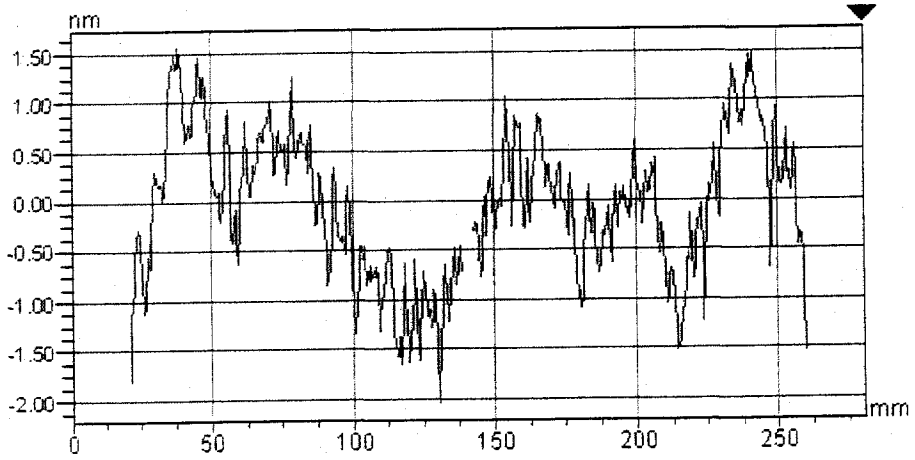

Transmission Data

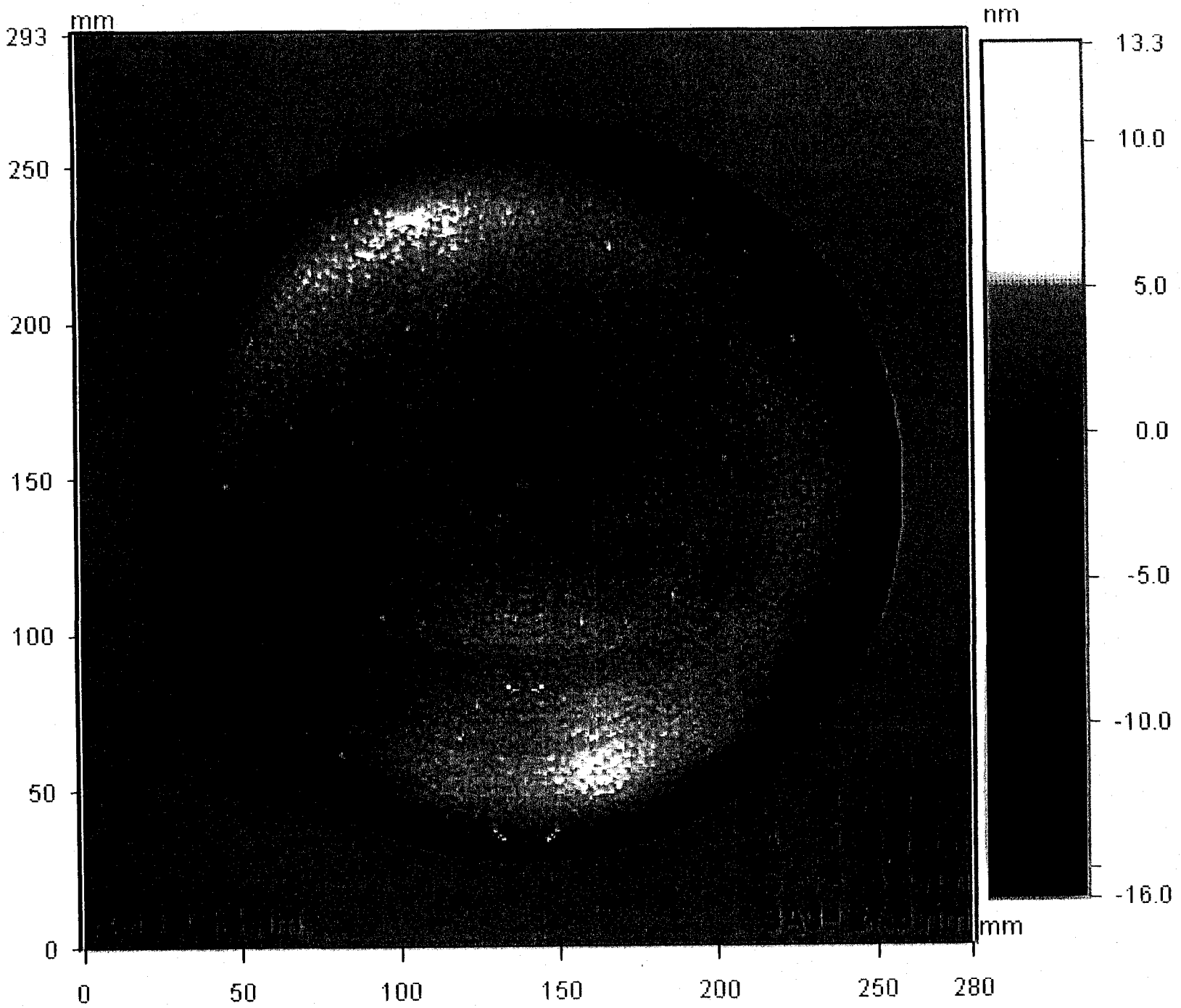

FIGURE